

Direct measurement of the magnetocaloric effect on micrometric Ni-Mn-(In,Sn) ribbons by the mirage effect under pulsed magnetic field

Cugini, F.; Orsi, D.; Brück, Ekkes; Solzi, M.

DOI

[10.1063/1.5061929](https://doi.org/10.1063/1.5061929)

Publication date

2018

Document Version

Final published version

Published in

Applied Physics Letters

Citation (APA)

Cugini, F., Orsi, D., Brück, E., & Solzi, M. (2018). Direct measurement of the magnetocaloric effect on micrometric Ni-Mn-(In,Sn) ribbons by the mirage effect under pulsed magnetic field. *Applied Physics Letters*, 113(232405). <https://doi.org/10.1063/1.5061929>

Important note

To cite this publication, please use the final published version (if applicable). Please check the document version above.

Copyright

Other than for strictly personal use, it is not permitted to download, forward or distribute the text or part of it, without the consent of the author(s) and/or copyright holder(s), unless the work is under an open content license such as Creative Commons.


Takedown policy

Please contact us and provide details if you believe this document breaches copyrights. We will remove access to the work immediately and investigate your claim.

Direct measurement of the magnetocaloric effect on micrometric Ni-Mn-(In,Sn) ribbons by the mirage effect under pulsed magnetic field

Cite as: Appl. Phys. Lett. **113**, 232405 (2018); <https://doi.org/10.1063/1.5061929>

Submitted: 24 September 2018 . Accepted: 12 November 2018 . Published Online: 05 December 2018

F. Cugini , D. Orsi, E. Brück, and M. Solzi



View Online



Export Citation



CrossMark

ARTICLES YOU MAY BE INTERESTED IN

[Inverse-direct magnetocaloric effect crossover in Ni₄₇Mn₄₀Sn_{12.5}Cu_{0.5} Heusler alloy in cyclic magnetic fields](#)

Applied Physics Letters **113**, 172406 (2018); <https://doi.org/10.1063/1.5049398>

[Large reversible magnetocaloric effect in Ni-Mn-In-Co](#)

Applied Physics Letters **106**, 021901 (2015); <https://doi.org/10.1063/1.4905371>

[Enhanced elastocaloric effect and cycle stability in B and Cu co-doping Ni-Mn-In polycrystals](#)

Applied Physics Letters **114**, 033901 (2019); <https://doi.org/10.1063/1.5080762>

Lock-in Amplifiers
up to 600 MHz



Watch



Direct measurement of the magnetocaloric effect on micrometric Ni-Mn-(In,Sn) ribbons by the mirage effect under pulsed magnetic field

F. Cugini,^{1,a)} D. Orsi,¹ E. Brück,² and M. Solzi^{1,3}

¹*Department of Mathematical, Physical and Computer Sciences, University of Parma, Parco Area delle Scienze 7/A, 43124 Parma, Italy*

²*Fundamental Aspects of Materials and Energy, Faculty of Applied Sciences, TU Delft Mekelweg 15, 2629 JB Delft, The Netherlands*

³*IMEM-CNR Institute, Parco Area delle Scienze 37/A, 43124 Parma, Italy*

(Received 24 September 2018; accepted 12 November 2018; published online 5 December 2018)

In this work, we report on the direct measurement of the magnetic field induced temperature change in a series of micrometric thick ribbons of Ni-Mn-In-Sn Heusler alloys, performed with an innovative experimental technique based on the thermo-optical “Mirage Effect.” The technique combines very fast measurement time, 1 T pulsed magnetic field in the millisecond range, and contactless temperature detection. These features make the technique ideal for the characterization of thin samples with a thickness down to a few micrometers. In this work, we demonstrate this by directly measuring the magnetocaloric effect (MCE) of micrometric-thick ribbons of Heusler alloys at the Curie transition, which was tuned on a wide temperature range by varying the Sn to In ratio. The direct test of the MCE in thin samples is fundamental for the development of refrigerant elements with a large heat-transfer coefficient and for the design of solid state micro devices for cooling and energy harvesting. *Published by AIP Publishing.* <https://doi.org/10.1063/1.5061929>

Magnetic refrigeration is a potentially very efficient and environmentally friendly technology to replace the current vapor-compression cycle based machines with a class of solid-state cooling devices.^{1,2} This technology exploits the magnetocaloric effect (MCE), which involves an entropy (ΔS_T) or a temperature change (ΔT_{ad}) of a magnetic material due to the variation of an applied magnetic field under isothermal or adiabatic conditions, respectively.³ By cyclic repetition of magnetization and demagnetization processes, a cooling cycle is realized. In the last few decades, research on magnetocaloric (MC) materials and on refrigeration machines has rapidly grown. Several prototypes have been realized, thus demonstrating the possibility to reach a high cooling power and efficiency at low noise levels.^{1,4}

Currently, a low working frequency is one of the main drawbacks that limit the specific cooling power and the energy-unit cost of magnetic cooling machines.^{5,6} In order to increase the working frequencies, it is necessary to decrease the time required for the heat-exchange between the magnetic active elements and a heat-transfer fluid.^{6,7} This task is pursued by designing active elements with a large thermal conductivity and high surface area to volume ratio (micrometric spheres, thin foils, and complex microstructures)^{1,8–12} or by proposing new heat-transfer mechanisms based on solid-state devices, such as thermal diodes.¹³ However, though the first solution is currently the most easily accessible, it brings along new problems for material synthesis and characterization. The characterization of bulk samples with the same nominal composition does not ensure a correct estimation of the MCE if such samples have different shapes and/or have been subjected to different synthesis and post-synthesis processes. Indeed, it was demonstrated that material processing routes can significantly alter the magnetic

and MC properties.^{14–17} This effect has to be particularly taken into consideration in the case of materials whose magnetic and MC properties are largely affected by stoichiometry and structural defects, impurities, chemical order, and microstructural details, as, e.g., in the case of Heusler alloys, rare-earth based materials, and FeRh alloys.^{14,18–22}

However, the direct measurement of the adiabatic temperature change, the driving force of cooling cycles, results in non-trivial problems in the case of thin or small samples. To perform correct ΔT_{ad} measurements, two main issues have to be accounted for: a low thermal mass of the temperature sensor, which must be negligible compared to that of the sample, and optimal adiabatic conditions.^{23,24} Common direct methods use thermocouples or resistive temperature sensors to perform measurements of temperature changes.^{23,25–27} These methods are hardly usable to measure thin and micro-structured samples due to their thermal mass and the difficulty to obtain a good thermal contact with the sample. A possible solution to this experimental difficulty, is to measure more samples together.^{28,29} However, this does not consider the contribution of the passive thermal mass due to the paste that is used to keep the samples together and possible small differences between the samples. Original solutions to directly measure the MCE in thin samples have been realized by exploiting thermo-acoustic methods or sensors for the optical detection of thermal radiation.^{24,30–33} However, these measurements generally utilize small modulated magnetic fields (<50 mT): thus, they do not allow to test materials response to the magnetic field changes really used in applications. Additionally, the results are not adequate in the case of hysteretic transitions.

Here, we present the direct characterization of a series of Ni-Mn-(In-Sn) ribbons performed with an innovative experimental setup based on the thermo-optical “Mirage Effect.” This technique, recently proposed,³⁴ allows the direct measurement of the adiabatic temperature change in

^{a)}Author to whom correspondence should be addressed: francesco.cugini@unipr.it

very thin materials and the test of their response to fast field changes (up to 700 T s^{-1}) with an amplitude of the magnetic field change up to 1 T. Indeed, this technique combines a short measurement time with the absence of a thermometer in contact with the sample, reducing heat losses from the sample during the measurement.

The studied materials belong to the family of (Ni,Mn)-based Heusler alloys that includes several interesting materials displaying considerable values of MCE at both a magnetostructural first-order phase-transition and at the Curie transition of the austenitic ferromagnetic phase.^{35–37} The possibility to easily tune both transitions with the composition, the absence of rare earths, the facility of production, and the high thermal conductivity make these alloys very promising for technological applications. In the present work, we study a series of alloys that originates from the $\text{Ni}_{50}\text{Mn}_{34}\text{In}_{16}$ composition, showing a considerable MCE at the Curie transition, slightly above room temperature.³⁶ The saturation magnetization of this material, about half that of Gd, is the maximum observed for this class of alloys showing a second-order transition near room temperature. The substitution of In by Sn drastically reduces the costs of the starting materials (more than 30 times) and gives the possibility to tune the transition temperature.

A series of 4 Heusler alloys, with the general formula $\text{Ni}_{50}\text{Mn}_{34}(\text{In}_{1-x}\text{Sn}_x)_{16}$ ($x = 0, 0.5, 0.75$, and 1; labelled: Sn0, Sn50, Sn75, and Sn100) were prepared in the form of ribbons by the melt-spinning technique. The Sn0 sample was prepared starting from a $\text{Ni}_{50}\text{Mn}_{34}\text{In}_{16}$ bulk sample synthesized by the arc-melting technique (details about the bulk sample preparation and its properties are reported in the [supplementary material](#)). The other 3 samples were prepared by melting the starting elements (99.99% purity) directly in the inductance oven of the melt-spinner. An excess of 1% Mn, In, and Sn was added to compensate for evaporation during melting. Later, the ribbons were sealed in quartz tubes under an Ar atmosphere, annealed for 2 h at 1073 K, and subsequently quenched in cold water. The compositions of the samples, measured through energy dispersive spectroscopy (EDS) microanalysis in a scanning electron microscope (SEM), are reported in Table I. An increase in the Ni content is observed with respect to the nominal composition. The very rapid quenching from the melt of the utilized synthesis method results in a crystalline microstructure characterized by elongated columnar grains perpendicularly oriented to the ribbon plane. These grains have a size ranging between a few micrometers and a few tens of micrometers (see SEM

TABLE I. Composition of the $\text{Ni}_{50}\text{Mn}_{35}(\text{In}_{1-x}\text{Sn}_x)_{15}$ alloys, determined by EDS analysis and expressed as at. %. The reported errors are the standard deviation estimated by mapping the composition on different points of the sample surface.

Sample	Composition (at. %)			
	Ni	Mn	In	Sn
Sn0	53.8 ± 0.4	31.2 ± 0.5	15.0 ± 0.1	...
Sn50	52.8 ± 0.4	32.7 ± 0.3	7.2 ± 0.1	7.3 ± 0.1
Sn75	54.2 ± 0.6	31.5 ± 0.7	3.5 ± 0.1	10.8 ± 0.2
Sn100	52.6 ± 0.4	33.0 ± 0.2	...	14.4 ± 0.2

TABLE II. Valence electron concentration per atom (e/a), lattice parameter of the cubic unit cell (c) at room temperature, saturation magnetization M_s , [* for Sn100, the saturation magnetization at 5 K of the austenitic phase was extrapolated from the $M(T)$ curve], Curie temperature (T_C), maximum isothermal entropy change (ΔS_T), and maximum adiabatic temperature change (ΔT_{ad}) in a $\mu_0 \Delta H = 1 \text{ T}$ for the four alloys.

	e/a	c (Å)	M_s ($\text{Am}^2 \text{kg}^{-1}$)	T_C (K)	ΔS_T ($\text{Jkg}^{-1} \text{K}^{-1}$)	ΔT_{ad} (K)
Sn0	8.014	6.00 ± 0.01	105.7 ± 0.9	287 ± 1	1.48 ± 0.08	0.81 ± 0.10
Sn50	8.077	5.99 ± 0.01	101.2 ± 0.5	304 ± 1	1.48 ± 0.08	0.78 ± 0.10
Sn75	8.162	5.99 ± 0.01	90.1 ± 0.5	317 ± 1	1.31 ± 0.11	0.66 ± 0.10
Sn100	8.146	6.01 ± 0.01	$87.0 \pm 0.7^*$	332 ± 1	1.29 ± 0.13	0.65 ± 0.10

images in the [supplementary material](#)). The average thickness of the ribbons is found to be about $8 \mu\text{m}$.

X-ray powder diffraction measurements, performed at room temperature using Cu $K\alpha$ radiation ($\lambda = 0.15418 \text{ nm}$) and reported in the [supplementary material](#), confirm the expected $L2_1$ (Fm3m) structure of austenite. The lattice parameter of the cubic structure, obtained from Rietveld refinement and reported in Table II, does not show a significant variation along the series of alloys.

Magnetization measurements have been performed using a Superconducting Quantum Interference Device (SQUID) magnetometer (MPMS XL of Quantum Design Inc.). The magnetic field was applied parallel to the ribbon surface, to minimize the effect of the demagnetizing field. Figure 1 shows the temperature dependence of magnetization for the alloys measured with an applied magnetic field of 0.01 T. All the alloys show a second order magnetic transition from a ferromagnetic to a paramagnetic state near room temperature. The Curie temperature (Table II) varies with the In to Sn ratio from 286.5 K (Sn0 sample) to 331.8 K (Sn100). On the contrary, their saturation magnetization progressively decreases with increasing Sn content (see Table II and [supplementary material](#)). All the samples show a ferromagnetic austenitic phase stable in a large temperature range around room temperature. Sample S100 presents, at low temperatures, a first-order structural transformation between the austenitic phase and a low-magnetization martensitic phase. The presence of the martensitic transformation sets a limit to the Mn content of the alloy. Indeed, a higher content of Mn,

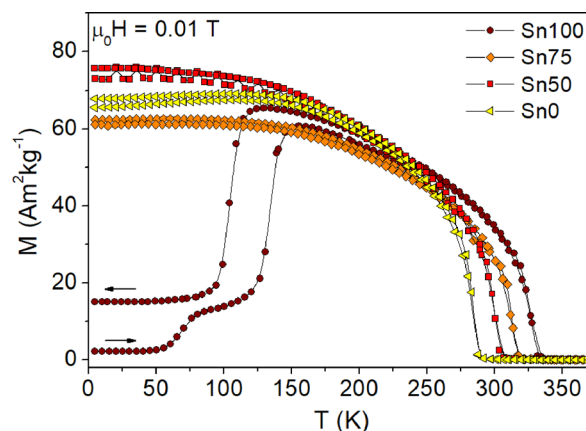


FIG. 1. Magnetization of the alloys as a function of temperature on heating and cooling with an applied magnetic field of 0.01 T.

at the expense of the (In-Sn) content, leads to an increase in the martensitic transformation temperature up to room temperature, with a resulting disappearance of the austenite Curie transition.^{38,39} In the case of studied samples, the martensitic transformation is still far away from room temperature and it does not affect the reported results at the Curie transition.

The observed structural and magnetic features of the samples are quite in agreement with those reported for bulk samples.^{14,36,38,39} A small reduction of the Curie temperature and of the saturation magnetization can be ascribed to an increase in the Ni/Mn ratio with respect to the stoichiometric composition. The opposite trends, with the Sn content, of T_C and of saturation magnetization derive from the complex magnetic configuration of Heusler alloys.

Isofield magnetic measurements at different applied magnetic fields were performed across the magnetic transition to obtain the isothermal entropy change using the Maxwell relation.³ Figure 2 shows the isothermal entropy change for the 4 alloys as a function of the temperature in $\mu_0\Delta H = 1$ T. The maximum value of Δs_T (Table II) follows a linear dependence with saturation magnetization. The Sn0 sample exhibits the maximum value, with a peak of $\Delta s_T = 1.48 \pm 0.08 \text{ J kg}^{-1} \text{ K}^{-1}$ at 286.3 K, quite in agreement with the bulk results.^{14,36}

The direct measurement of the adiabatic temperature change was performed by the non-contact experimental setup presented in Ref. 34. This instrument is based on the thermo-optical mirage effect, which consists in the deflection of a light beam by a thermal gradient. In the developed experimental setup (sketched in Fig. 3), a laser beam, grazing the sample surface, is deflected by the temperature gradient that is formed in the thin air layer overlying the sample surface due to a temperature change of the sample. The MCE is induced in the sample by a pulsed magnetic field with a maximum amplitude of 1 T and a period of the order of a few milliseconds. It was demonstrated that the thermal diffusion time to the gas layer next to the sample surface is fast enough to probe the material's magnetocaloric response to short pulses of the order of milliseconds.³⁴ This fast response time and the limited heat capacity of the gas layer ensure that we can consider the change in temperature to be adiabatic. The angle of deflection of the laser beam (Φ), with respect to the sample surface, is proportional to the

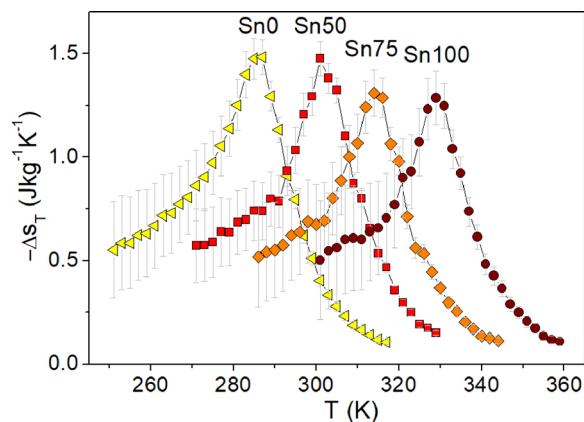


FIG. 2. Isothermal entropy change of the ribbons as a function of temperature, calculated for $\mu_0\Delta H = 1$ T from isofield $M(T)$ measurements by using the Maxwell equation.

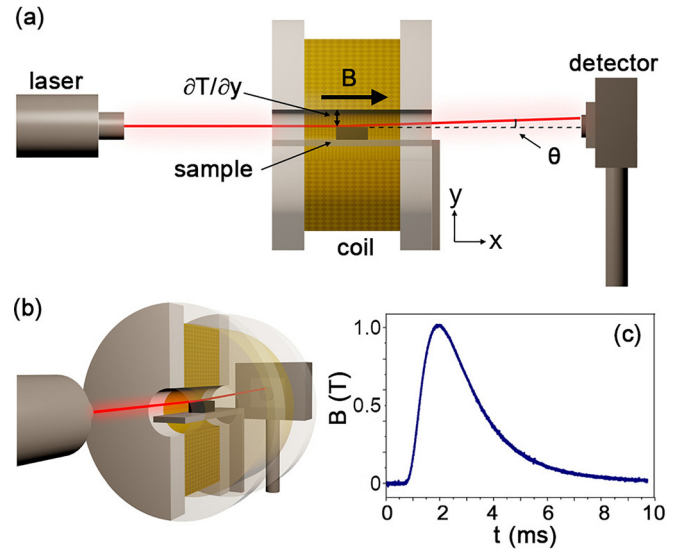


FIG. 3. Sketch of the experimental setup for the direct measurement of the adiabatic temperature change. (c): Time profile of the magnetic field pulse.

temperature gradient $[\partial T(y, t)/\partial y]$, the refractive index of the deflecting medium (n , in this case of air), the temperature coefficient of the refractive index (dn/dT), and the length of the laser path (d) across the temperature gradient⁴⁰

$$\Phi(t) = \frac{1}{n} \frac{dn}{dT} \frac{\partial T(y, t)}{\partial y} d. \quad (1)$$

In our case, d corresponds to the sample length since each part of the sample experiences the same temperature change. By measuring the deflection of the laser beam and by calibrating the setup with a reference material (gadolinium), it is possible to obtain the absolute temperature change induced in the sample by the applied magnetic field.³⁴

Figure 4 reports the adiabatic temperature change measured as a function of temperature for the alloys by using a pulsed magnetic field with an amplitude of 1 T and a characteristic time of 1.3 ms. ΔT_{ad} shows a small decrease with substitution of In by Sn, from $\Delta T_{ad} = 0.8 \pm 0.1$ K for the In-sample (Sn0) to $\Delta T_{ad} = 0.6 \pm 0.1$ K for the Sn-sample (Sn100), following the behavior of the isothermal entropy change with composition. The maximum value recorded for the In-sample is lower than that of the corresponding bulk sample

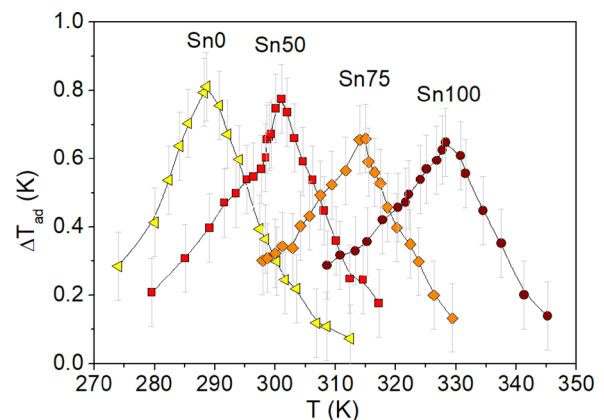


FIG. 4. Adiabatic temperature change of the ribbons as a function of temperature induced by a magnetic field pulse with an amplitude of 1 T.

($\Delta T_{ad} = 1.0 \pm 0.1$ K, [supplementary material](#)), accordingly to the reduction of the saturation magnetization. The shape and the width of the $\Delta T_{ad}(T)$ curves are the same for all the samples and are comparable with those of the starting bulk alloy and of Gd. A comparison of the curves, normalized to their maximum value, is reported in the [supplementary material](#). All the curves collapse on the same, as predicted for MCE across a second-order transformation.⁴¹

In conclusion, this paper reports on the direct measurement of the adiabatic temperature change of 4 melt-spun ribbons of Heusler alloys induced by a pulsed magnetic field of 1 T amplitude and 1.3 ms characteristic time. The obtained results demonstrate the possibility to easily tune, with varying composition, the peak of the MCE across the second-order transformation, and thus to realize with these materials high-performance thin-layered cooling elements. The high thermal conductivity of these metallic alloys and the possibility to realize thin foils, promote the realization of cooling elements with high heat-exchange coefficients. However, the low value of maximum MCE still limits the application of these materials in efficient devices. An increase in the saturation magnetization together with a reduction of the transition temperature could bring along an effective use of these alloys as active elements in magnetic refrigerators.

From the instrumental point of view, the suitability of the presented experimental setup based on the Mirage Effect, was demonstrated to correctly and easily perform direct magnetocaloric characterization of thin samples with a magnetic field change really used in prototypes of magnetic refrigerators. This experimental setup might be particularly useful for the test of the MC response to fast field changes ($\mu_0 dH/dt > 700$ Ts⁻¹) of thin materials showing a giant-MCE related to a first-order magnetic transition [e.g., Heusler alloys with a martensitic transition, Gd₅(Si,Ge)₄, FeRh, Fe₂P-based compounds, and La(Fe,Si)₁₃ compounds].⁴² Moreover, the use of this technique can be extended in principle also to measure electrocaloric and elastocaloric materials: the absence of a temperature sensor in contact with the sample reduces drawbacks due to high voltages or mechanical stresses.

See [supplementary material](#) for the magnetic and MC characterization of the SnO bulk sample and for further magnetic, structural, and microstructural data of the Heusler ribbons.

F. Cugini acknowledges Dr. X. F. Miao and Dr. M. F. J. Boeije for the useful discussions, Ing. A. J. E. Lefering and Dr. K. Goubitz for the technical support, and the entire group FAME (TU Delft) for the hospitality and support. This work was financially supported by Fondazione Cariparma.

¹A. Kitanovski, J. Tušek, U. Tomc, U. Plaznik, M. Ožbolt, and A. Poredoš, *Magnetocaloric Energy Conversion, From Theory to Applications* (Springer I, 2015).

²D. J. Silva, B. D. Bordalo, A. M. Pereira, J. Ventura, and J. P. Araújo, *Appl. Energy* **93**, 570 (2012).

³A. M. Tishin and Y. I. Spichkin, *The Magnetocaloric Effect and Its Applications* (CRC Press, 2003).

⁴B. Yu, M. Liu, P. W. Egolf, and A. Kitanovski, *Int. J. Refrig.* **33**, 1029 (2010).

⁵K. K. Nielsen and K. Engelbrecht, *J. Phys. D: Appl. Phys.* **45**, 145001 (2012).

⁶D. J. Silva, B. D. Bordalo, J. Puga, A. M. Pereira, J. Ventura, J. C. R. E. Oliveira, and J. P. Araújo, *Appl. Therm. Eng.* **99**, 514 (2016).

⁷G. Porcari, K. Morrison, F. Cugini, J. A. Turcaud, F. Guillou, A. Berenov, N. H. Van Dijk, E. H. Brück, L. F. Cohen, and M. Solzi, *Int. J. Refrig.* **59**, 29 (2015).

⁸J. D. Moore, D. Klemm, D. Lindackers, S. Grasemann, R. Träger, J. Eckert, L. Löber, S. Scudino, M. Katter, A. Barcza, K. P. Skokov, and O. Gutfleisch, *J. Appl. Phys.* **114**, 043907 (2013).

⁹B. Weise, K. Sellschopp, M. Bierdel, A. Funk, M. Bobeth, M. Krautz, and A. Waske, *J. Appl. Phys.* **120**, 125103 (2016).

¹⁰J. Tušek, A. Kitanovski, S. Zupan, I. Prebil, and A. Poredoš, *Appl. Therm. Eng.* **53**, 57 (2013).

¹¹I. A. Radulov, D. Y. Karpenkov, K. P. Skokov, A. Y. Karpenkov, and T. Braun, *Acta Mater.* **127**, 389 (2017).

¹²A. K. Sellschopp, B. Weise, M. Krautz, F. Cugini, M. Solzi, L. Helmich, A. Hütten, and A. Waske, *Energy Technol.* **6**, 1448 (2018).

¹³U. Tomc, J. Tušek, A. Kitanovski, and A. Poredoš, *Appl. Therm. Eng.* **58**, 1 (2013).

¹⁴F. Cugini, L. Righi, L. Van Eijck, E. Brück, and M. Solzi, *J. Alloys Compd.* **749**, 211 (2018).

¹⁵S. V. Taskaev, M. D. Kuz'min, K. P. Skokov, D. Y. Karpenkov, A. P. Pellenen, V. D. Buchelnikov, and O. Gutfleisch, *J. Magn. Magn. Mater.* **331**, 33 (2013).

¹⁶S. Taskaev, K. Skokov, D. Karpenkov, V. Khovaylo, M. Ulyanov, D. Bataev, A. Dyakonov, A. Fazlitdinova, and O. Gutfleisch, *J. Magn. Magn. Mater.* **442**, 360 (2017).

¹⁷S. Taskaev, K. Skokov, V. Khovaylo, M. Ulyanov, D. Bataev, D. Karpenkov, I. Radulov, A. Dyakonov, and O. Gutfleisch, *J. Magn. Magn. Mater.* **459**, 46 (2018).

¹⁸A. L. Alves, E. C. Passamani, V. P. Nascimento, A. Y. Takeuchi, and C. Larica, *J. Phys. D: Appl. Phys.* **43**, 345001 (2010).

¹⁹V. Recarte, J. I. Perez-Landazabal, V. Sanchez-Alarcos, and J. A. Rodriguez-Velamazán, *Acta Mater.* **60**, 1937 (2012).

²⁰F. Cugini, G. Porcari, T. Rimoldi, D. Orsi, S. Fabbri, F. Albertini, and M. Solzi, *JOM* **69**, 1422 (2017).

²¹V. I. Zverev, A. M. Tishin, Z. Min, Y. Mudryk, K. A. Gschneidner, Jr., and V. K. Pecharsky, *J. Phys.: Condens. Matter.* **27**, 146002 (2015).

²²V. I. Zverev, A. M. Saletsky, R. R. Gimaev, A. M. Tishin, T. Miyayama, and J. B. Staunton, *Appl. Phys. Lett.* **108**, 192405 (2016).

²³G. Porcari, M. Buzzi, F. Cugini, R. Pellicelli, C. Pernechele, L. Caron, E. Brück, and M. Solzi, *Rev. Sci. Instrum.* **84**, 073907 (2013).

²⁴F. Cugini, G. Porcari, and M. Solzi, *Rev. Sci. Instrum.* **85**, 074902 (2014).

²⁵S. Y. Dan'kov, A. M. Tishin, V. K. Pecharsky, and K. A. Gschneidner, *Rev. Sci. Instrum.* **68**, 2432 (1997).

²⁶J. Kamarád, J. Kaštil, and Z. Arnold, *Rev. Sci. Instrum.* **83**, 083902 (2012).

²⁷K. P. Skokov, V. V. Khovaylo, K.-H. Mueller, J. D. Moore, J. Liu, and O. Gutfleisch, *J. Appl. Phys.* **111**, 07A910 (2012).

²⁸J. Y. Law, V. Franco, and R. V. Ramanujan, *J. Appl. Phys.* **110**, 023907 (2011).

²⁹C. O. Aguilar-Ortiz, J. P. Camarillo-Garcia, J. Vergara, P. SiAlvarez-Alonso, D. Salazar, V. A. Chernenko, and H. Fores-Zuniga, *J. Alloys Compd.* **748**, 464 (2018).

³⁰B. R. Gopal, R. Chahine, M. Földeák, and T. K. Bose, *Rev. Sci. Instrum.* **66**, 232 (1995).

³¹A. O. Guimarães, M. E. Soffner, A. M. Mansanares, A. A. Coelho, A. Magnus, G. Carvalho, M. J. M. Pires, S. Gama, and E. C. da Silva, *Phys. Rev. B* **80**, 134406 (2009).

³²D. V. Christensen, R. Bjork, K. K. Nielsen, C. R. H. Bahl, A. Smith, and S. Clausen, *J. Appl. Phys.* **108**, 063913 (2010).

³³J. Döntgen, J. Rudolph, A. Waske, and D. Hägele, *Rev. Sci. Instrum.* **89**, 033909 (2018).

³⁴F. Cugini, G. Porcari, C. Viappiani, L. Caron, A. O. Santos, L. P. Cardoso, E. C. Passamani, J. R. C. Proveti, S. Gama, E. Brück, and M. Solzi, *Appl. Phys. Lett.* **108**, 012407 (2016).

³⁵J. Liu, T. Gottschall, K. P. Skokov, J. D. Moore, and O. Gutfleisch, *Nat. Mater.* **11**, 620 (2012).

³⁶S. Singh, L. Caron, S. W. D. Souza, T. Fichtner, G. Porcari, S. Fabbri, C. Shekhar, S. Chadov, M. Solzi, and C. Felser, *Adv. Mater.* **28**, 3321 (2016).

³⁷T. Krenke, E. Duman, M. Acet, E. F. Wassermann, X. Moya, L. Mañosa, and A. Planes, *Nat. Mater.* **4**, 450 (2005).

³⁸T. Krenke, M. Acet, E. F. Wassermann, X. Moya, L. Mañosa, and A. Planes, *Phys. Rev. B* **73**, 174413 (2006).

³⁹A. Çakır, L. Righi, F. Albertini, M. Acet, and M. Farle, *Acta Mater.* **99**, 140 (2015).

⁴⁰J. Zhou, J. Zhao, and J. Shen, *J. Opt. Soc. Am. B* **22**, 2409 (2005).

⁴¹V. Franco and A. Conde, *Int. J. Refrig.* **33**, 465 (2010).

⁴²V. V. Khovaylo, V. V. Rodionova, S. N. Shecyrtaov, and V. Novosad, *Phys. Status Solidi B* **251**, 2104 (2014).